Environmental Science and Ecotechnology 29 (2026) 100651

Contents lists available at ScienceDirect

Environmental Science and Ecotechnology

journal homepage: www.journals.elsevier.com/environmental-science-and-ecotechnology/

Original Research

Selective eradication of pathogenic bacteria using amine-modified corn-straw carbon dots

Pengzhao Lv [a], Yu Jiang [a], Jialin Wang [a], Yige Shi [a], Zhengda Lin [a], Duo Wei [b,*], Wei Zuo [a], Jun Zhang [a,**]

[a] State Key Lab of Urban Water Resource and Environment, National Engineering Research Center for Safe Disposal and Resource Recovery of Sludges, School of Environment, Harbin Institute of Technology, Harbin, 150001, China
[b] State Key Laboratory of Space Power-Sources, School of Chemistry and Chemical Engineering, Harbin Institute of Technology, Harbin, 150001, China

ARTICLE INFO

Article history:
Received 13 June 2025
Received in revised form
24 December 2025
Accepted 24 December 2025

Keywords:
Corn straw
Carbon dots
Staphylococcus aureus
Selective killing
Oxidase

ABSTRACT

The rise of antimicrobial resistance and the ecological harm inflicted by broad-spectrum disinfectants underscore the urgent need for species-specific strategies that eradicate pathogenic bacteria without disrupting beneficial microbial communities. *Staphylococcus aureus* thrives in diverse aquatic environments across wide temperature ranges, posing persistent risks to human health and exacerbating resistance challenges, yet existing agents lack the precision to target this pathogen selectively. Here we show that triethylenetetramine-functionalized carbon dots, derived from corn straw biomass via one-step hydrothermal synthesis, exhibit intrinsic oxidase-like activity that selectively eliminates *S. aureus*. These nanomaterials achieve complete bactericidal efficacy (100%) against *S. aureus* at 50 μg mL^{-1} within 1 h at 37 °C, retaining robust activity (80%) even at 4 °C, through synergistic preferential binding to cell-wall polysaccharides—facilitated by retained biomass cellulose moieties—combined with membrane disruption and generation of superoxide radicals ($\cdot O_2^-$) and singlet oxygen ($^1O_2$). This selectivity spares *Bacillus subtilis* and Gram-negative species such as *Escherichia coli* and *Pseudomonas aeruginosa*, owing to differences in cell-wall architecture and reduced affinity. Amine chain length tunes the oxidase-mimicking potency, enabling oxygen-dependent reactive oxygen species production without external stimuli. By upcycling abundant agricultural waste into rapidly photodegradable (within 11 days under visible light) precision disinfectants, this approach provides a sustainable way for ecologically compatible pathogen control, advancing rational design principles for next-generation nano-antimicrobials.

1. Introduction

Staphylococcus aureus (*S. aureus*) shows extraordinary adaptability to many environments, including human skin [1], food [2], garbage [3], wastewater treatment plants [4], public spaces [5], and households [6]. Infections caused by *S. aureus* are becoming increasingly widespread, and the development of antimicrobial resistance in *S. aureus* is becoming a significant threat to global public health [7,8]. Data from the China Antimicrobial Surveillance Network in 2023 showed that the detection rate of *S. aureus* ranked third among the major clinical isolates, accounting for 9.23% of total samples. In recent years, *S. aureus* bioaerosols in sewage plants have been found to have an extremely adverse impact on human health [9]. Vantarakis et al. [10] tested the bacterial flora near wastewater treatment plants and found that of 83 randomly detected bacterial isolates, 29% (24 strains) were *S. aureus*. Other studies have found that *S. aureus* bioaerosols are the main cause of chronic lung infections [11].

S. aureus can survive in freshwater, river water, and seawater, and even survive for a long time in cold, nutrient-rich saltwater [12]. This presents a major challenge in the development of materials with high antimicrobial activity that can adapt to different water bodies at varying temperatures for public health protection [13]. Existing conventional antibacterial agents (e.g., metal ions

* Corresponding author.
** Corresponding author.
E-mail addresses: DuoWei@catalysis.email.cn (D. Wei), hitsunyboy@126.com (J. Zhang).

https://doi.org/10.1016/j.ese.2025.100651

[14], quaternary ammonium compounds [15], and antibiotics [16]) face challenges such as high costs, complex synthesis processes, antibiotic resistance, and environmental pollution [17]. As an emerging carbon-based nanomaterial, carbon dots (CDs) have garnered growing interest due to their remarkable antibacterial properties [18,19]. For instance, Wang et al. [20] revealed that amine-modified CDs can generate reactive oxygen species (ROS) via peroxidase- and oxidase-mimicking activities. Their low drug resistance potential and good biocompatibility make them promising alternatives to traditional antibiotics. However, despite the extensive biological applications reported, the precise bactericidal mechanisms of CDs remain unclear and controversial.

In the circular economy framework, leveraging biomass waste as a carbon source for synthesizing value-added CDs addresses resource limitations and expands their practical applications through sustainable production [21,22]. Current research on biomass-derived CDs is still in the preliminary stages, with existing studies mainly focusing on the antibacterial properties of high-value biomass, such as the Chinese herbal medicine forsythia [23], turmeric [24], and garlic [25], while the antibacterial potential of cheap and abundant biomass waste, such as corn straws, remains under investigated. Inspired by previous research [26], we utilized amine modifiers with varying active hydrogen densities (e.g., ethylenediamine [EDA], diethylenetriamine [DTEA], and triethylenetetramine [TETA]) to investigate the antibacterial properties of CDs. Most existing antibacterial studies are conducted at the optimal bacterial growth temperature (37 °C), with limited data on room temperature (25 °C) or low temperatures (4–15 °C). Thus, utilizing low-cost biomass such as corn stalks to synthesize amine-modified CDs and exploring their disinfection performance in real water matrices (especially under low-temperature conditions) carries considerable scientific and practical relevance.

In this study, a systematic evaluation of the antibacterial properties of a series of amine-modified biomass waste corn straw CDs was conducted, focusing on the effects of amine-modified reagents on the antibacterial activity of the biomass CDs. The selective antibacterial activity of the CDs against *S. aureus* was assessed at various CD concentrations (10–200 μg mL^{-1}), at different temperatures (4–37 °C), and in real water matrices. The selective antibacterial mechanisms of TETA CDs were revealed through a series of characterization tests.

2. Materials and methods

2.1. Materials and chemical reagents

Corn straw powder (100 mesh; cellulose, 32.4%; hemicellulose, 19.2%; and lignin, 19.5%) was obtained from the farmers' market in Nangang District, Harbin, China. The strains of *Staphylococcus aureus* (*S. aureus*, ATCC 6538), *Escherichia coli* (*E. coli*, ATCC 25922), *Pseudomonas aeruginosa* (*P. aeruginosa*, ATCC 15692), and *Bacillus subtilis* (*B. subtilis*, ATCC 6633) were obtained from Beijing Microbiological Culture Collection Center (Beijing, China). Ascorbic acid (AA; 99%), EDA (99%), DTEA (99%), TETA (70%), sodium alginate (SA), propidium iodide (PI; 98%), and 2′,7′-dichlorodihydrofluorescein diacetate (DCFH-DA; 97%) were obtained from Aladdin (Shanghai, China). Phosphatidyl ethanolamine (PE) was obtained from Macklin (Shanghai, China), and bovine serum was obtained from the Beyotime Institute of Biotechnology (Shanghai, China). SYBR Green I (10,000 × concentrate in dimethyl sulfoxide) was obtained from Thermo Fisher Scientific, USA. Phosphate-buffered saline (PBS; pH 7.4) and normal saline (NS; 0.9% w/v) were used to mimic physiological conditions. Dulbecco's Modified Eagle Medium (DMEM) was obtained from Corning (Corning, NY, USA). Mouse embryo fibroblasts (NIH 3T3) and fetal bovine serum were obtained from Procell Life Science & Technology Co., Ltd. (Wuhan, China). Cell Counting Kit-8 (CCK-8) was obtained from Invigentech (Irvine, CA, USA).

2.2. Syntheses of a series of CDs

We prepared amine-modified CDs using a simple one-step hydrothermal method. Corn straw powder (1 g) was dispersed in deionized water (25 mL) and combined with different amine sources (EDA, DTEA, and TETA), then sonicated for 30 min. The suspension was transferred to a polytetrafluoroethylene-lined autoclave and subjected to hydrothermal treatment at 160 °C for 8 h. Following the reaction, the mixture was sonicated for 30 min to ensure homogeneity and centrifuged at 10,000 rpm for 30 min to remove insoluble residues. The CD solution was then transferred into a dialysis bag (Molecular Weight Cutoff: 500 Da) and dialyzed in deionized water for 24–36 h until the dialysis solution was clear. Finally, the CD powder was obtained by vacuum freeze-drying for subsequent experiments. Samples prepared with EDA, DTEA, and TETA were named EDA CDs, DTEA CDs, and TETA CDs, respectively, whereas CDs prepared with deionized water without amine sources were named CS CDs.

2.3. Material characterization

The morphological characteristics of the CDs were examined by a high-resolution transmission electron microscope (HRTEM; Talos F200S G2, FEI, USA) operated at 200 kV. Fourier transform infrared (FTIR) absorption spectra were collected using a Frontier FTIR spectrometer (PerkinElmer, USA). X-ray photoelectron spectroscopy (XPS; Kratos Analytical, UK) was carried out to analyze the surface chemical states and elemental valences. The crystalline phase analysis was conducted using an X-ray diffractometer (Bruker D8 Advantage, Germany). The electron paramagnetic resonance (EPR) spectra were acquired using 5,5-dimethyl-1-pyrroline N-oxide (DMPO) and 2,2,6,6-tetramethylpiperidine (TEMP) as trapping agents on an EPR spectrometer (Bruker BioSpin EMXplus-6/1, Germany). The bacterial structure and morphology were characterized using scanning electron microscopy (SEM; ZEISS SIGMA 500, Zeiss, Germany) and transmission electron microscopy (TEM; H-7650, Hitachi, Japan). The zeta potential was characterized using a ZETA potential analyzer (Anton Paar Litesizer50, Austria). The fluorescence signals of bacteria were detected by a Confocal laser scanning microscope (CLSM; ZEISS LSM800, Germany). The leakage of potassium ions (K^+) was quantitatively detected by Inductively Coupled Plasma Optical Emission Spectrometry (ICP-OES; PerkinElmer Avio 550 Max, USA). The optical properties of the CDs were characterized by an ultraviolet spectrophotometer (UV–Vis; SHIMADZU UV-2550, Japan).

2.4. Antibacterial activity experiments

We evaluated the narrow-spectrum, selective antibacterial activity of a series of amine-modified corn straw CDs against the pathogenic bacterium *S. aureus* and the probiotic bacterium *B. subtilis* by assessing differences in their antibacterial efficacy [27]. Bacterial strains were cultured overnight in lysogeny broth (LB) to prepare them for subsequent experiments. Specifically, *S. aureus* and *B. subtilis* were incubated in LB broth at 37 °C for 12 h. Prior to each experiment, all vessels and different water samples were autoclaved at 121 °C for 20 min. A series of concentrations of CDs was prepared and added to suspensions containing *S. aureus* and *B. subtilis* (~10^5 CFU mL^{-1}), with a total volume kept at 2 mL, then the mixtures were allowed to incubate at 37 °C for different

times, and the samples without CD treatment were treated identically to the control group. Then, 10 μL of the diluted bacterial solution was uniformly applied to the surface of the LB agar plate and cultured for 12–16 h at 37 °C. Finally, colony-forming units (CFUs) were counted to determine the antibacterial rate. Each test was performed in triplicate. The antibacterial rate of the series of CDs was calculated as follows:

$$A = \frac{N_b - N_s}{N_b} \times 100\%$$

where A is the antibacterial rate of CDs, N_b is the number of CFUs on LB agar plates of the blank control, and N_s represent the number of CFUs in the groups treated with the series of CDs. The analytical methods and characterization are described in more detail in Supplementary Texts S1–S7.

3. Results and discussion

3.1. Synthesis and characterization of materials

The series of CDs was successfully prepared through a bottom-up one-step hydrothermal method, which hydrothermally carbonized biomass to carbonized polymer dots [28] and endowed CDs with different amine functional groups through different amine modifiers (EDA, DTEA, and TETA). Compared to the direct hydrothermal carbonization of biomass, the addition of amine modifiers significantly increased the CD yield. The series of CDs exhibited good aqueous dispersion behavior and features spherical nanoparticles with diameters ranging from 1 to 4 nm (mean: 2–3 nm) with homogeneous distribution (Fig. 1a–d) [29]. The HRTEM images indicated that the lattice spacing of the series of CDs was approximately 0.21 nm, corresponding to the (100) plane in the typical graphite lattice structure, which is not clearly visible, suggesting low crystallinity and properties of amorphous carbon (Fig. 1a–d) [30]. The diffraction pattern of TETA CDs revealed a dominant peak at 13° (attributed to the (100) plane of graphene oxide) and two minor peaks at 30° and 42° (corresponding to the (002) and (101) planes of graphite) (Fig. 1e) [31]. The reduced peak intensities and broadened full width at half maximum suggest the formation of an amorphous carbon structure. These findings confirmed the poorly crystalline, heterogeneous multi-layered structure of TETA CDs, consistent with previous reports on CD properties [32].

Given that surface functional groups serve as critical determinants of antimicrobial activity, FTIR and XPS were employed to characterize the CDs. FTIR spectra of the raw material and the CD series (Fig. 1f) show that the CDs largely retain the functional groups of the raw corn straw. Corn straw contains a large amount of lignin, cellulose, and hemicellulose; all of these biopolymers contain abundant methylene (–CH_2–) and hydroxyl (–OH) functional groups, as reflected by the characteristic FTIR absorption bands at 2920 cm^{-1} (asymmetric CH_2 stretching), 2850 cm^{-1} (symmetric CH_2 stretching), and 3429 cm^{-1} (–OH stretching) [33,34]. The cellulose-specific peaks were observed at 1376 cm^{-1} (C–H bending in CH_2 groups) and 1062 cm^{-1} (C–O stretching in primary alcohols), which overlapped with C–N stretching at 1059 cm^{-1} [35] and 890 cm^{-1} (β-glycosidic linkage vibration), confirming the presence of intact cellulose moieties [34]. The peak at 1632 cm^{-1} was attributed to O-H bending vibrations of adsorbed water molecules in cellulose [33,36].

Significantly, the characteristic hemicellulose peaks at 1730 cm^{-1} (C=O stretching of the ferulic and p-Coumaric acids) and lignin peaks at 1510 cm^{-1} (aromatic C=C stretching of the benzene ring) and 1247 cm^{-1} (C=O in lignin) vanished after amine modification [36–38]. This suggests a preferential reaction of amine groups with ester linkages in the hemicellulose and carboxylic groups in lignin, as well as Schiff base formation with carbonyl groups on the CD surface [39]. The N–H bonds in amino groups and C=N bonds in the series of amine-modified CDs overlap with OH stretching at 3429 and 1632 cm^{-1}, respectively [40,41].

We used XPS to characterize the surface chemistry of amine-modified CDs. The survey spectrum (Fig. 1g) revealed a notable increase in nitrogen content from 2.9% (CS CDs) to 4.1% (EDA CDs), 3.3% (DTEA CDs), and 5.6% (TETA CDs), confirming successful amine doping. High-resolution C 1s spectra (Fig. 1h) displayed characteristic peaks at 284.8 eV (C–C), 286.3 eV (C–O/C–N), and 288.2 eV (C=O/C=N), consistent with previous reports [42,43]. And the ratio of C=O/C=N in TETA CDs increased significantly, and the N content of different CDs increased gradually with the extension of the carbon chain of the modifier. This is consistent with the report of Niu et al. [44]. The O 1s spectra (Fig. 1i) indicated that the control CS CDs contained two distinct components: a low-binding-energy peak at 531.1 eV (C=O) and a higher-energy peak at 532.74 eV (C–OH/C–O–C). The series of amine-modified corn straw CDs exhibited a new peak at around 535 eV (O–C=O), further supporting the presence of oxygen-containing functional groups [45].

These results indicate that amine modification introduces nitrogen moieties while retaining the oxygen-rich surface chemistry of biomass-derived CDs [46]. In contrast to the CS CDs (Fig. 1j), which exhibited a single peak at 400.1 eV corresponding to C–N bonds, the amine-modified CDs displayed two distinct peaks at 399.6 eV and 402.0 eV, which can be attributed to C=N and N-H bonds, respectively [47]. These results indicate that the primary amines of the three amine modifiers underwent a Schiff base reaction with C=O to form C=N bonds [48]. Notably, the new peak appearing around 402 eV is usually reported as a positively charged amine [49]. The percentages of the functional groups in high-resolution XPS are shown in Table 1. Combined with the FTIR analysis, it was shown that the amine modifiers were successfully modified onto the surface of the CD [50].

3.2. Antibacterial effects of amine-modified CDs

The antibacterial efficacy of CDs was systematically evaluated using model Gram-positive bacteria *S. aureus* and *B. subtilis* and Gram-negative bacteria *E. coli* and *P. aeruginosa* as controls [13]. First, CDs prepared with corncob [51], corn straw [30], moso bamboo [52], and chlorella vulgaris [53] as the carbon sources were used to test the antibacterial properties against *S. aureus*. Corn straw CDs with EDA as the amine modifier (EDA CDs) had significant antibacterial activity at a concentration of 100 μg mL^{-1}, eliminating approximately 10^5 CFUs of *S. aureus* within 1 h (Supplementary Fig. S1). The antibacterial efficacy of EDA CDs was evaluated in a dose-dependent manner against the Gram-positive pathogen *S. aureus* and the probiotic bacterium *B. subtilis* at an initial density of 10^5 CFU mL^{-1} (Fig. 2a). Notably, EDA CDs demonstrated robust bactericidal activity against *S. aureus*, achieving ≥99% bacterial reduction at concentrations as low as 50 μg mL^{-1}.

In contrast, even at the highest tested concentration (4 mg mL^{-1}) of TETA CDs, no observable growth inhibition of *B. subtilis* was detected (Supplementary Fig. S2), a feature more significant than the previously reported selective antibacterial concentration 392.85 μg mL^{-1} of CuO nanoparticles, indicating that the amine-modified CDs exhibit excellent selective antibacterial activity [27]. We observed a clear dose- and chain-length-dependent antibacterial effect (Fig. 2b). The bactericidal efficacy of the CDs improved as the concentration of the CDs increased and

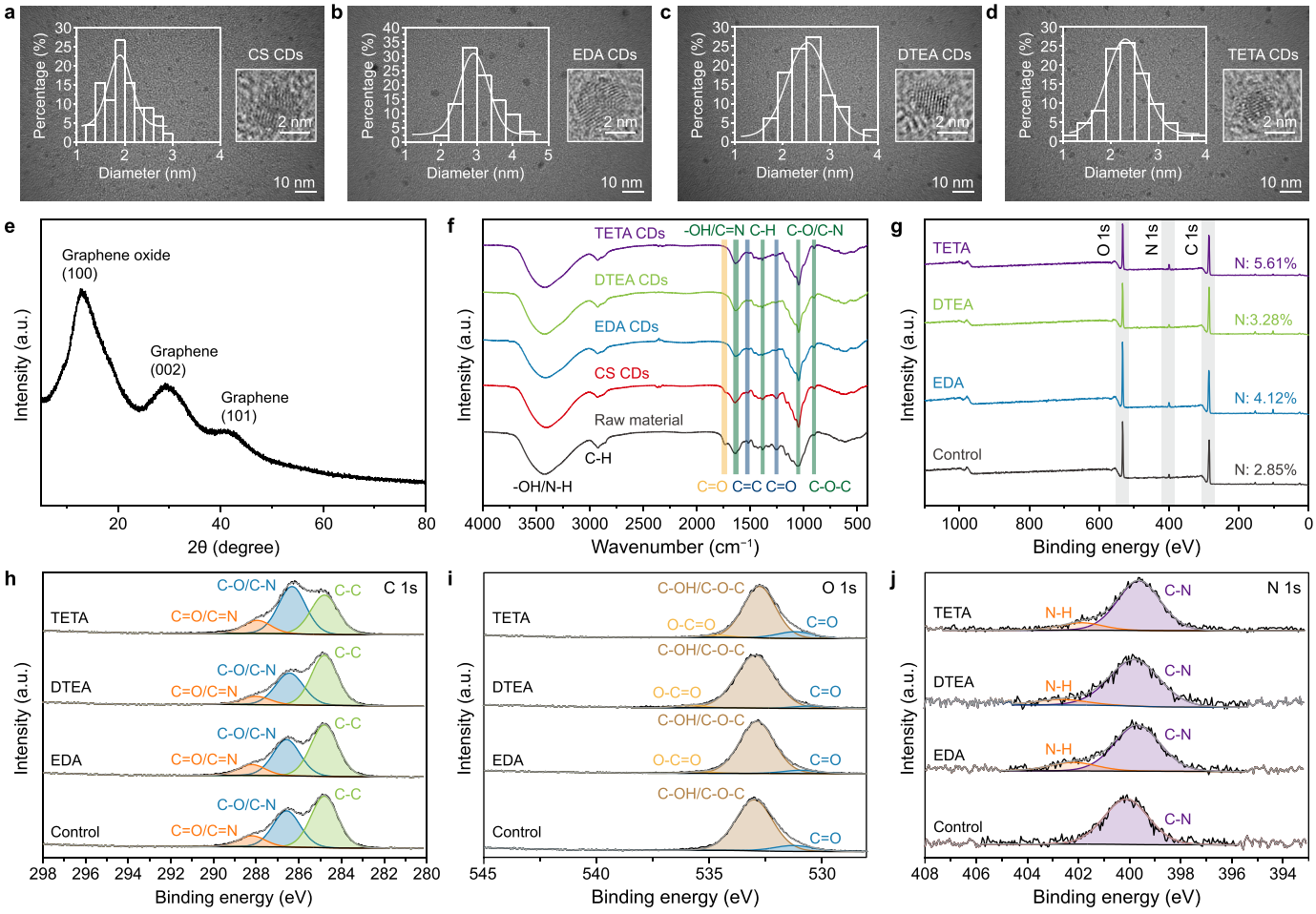

Fig. 1. **a**–**d**, Transmission electron microscopy images and particle-size distributions (left insert) of a series of carbon dots (CDs): CS CDs (**a**), EDA CDs (**b**), DTEA CDs (**c**), TETA CDs (**d**). **e**, X-ray diffraction patterns of TETA CDs. **f**, Fourier transform infrared spectra of the raw material and a series of CDs. Yellow shading, hemicellulose; green shading, cellulose; blue shading, lignin. **g**, X-ray photoelectron spectroscopy (XPS) survey spectra. **h**–**j**, High-resolution XPS spectra of C 1s (**h**), O 1s (**i**), and N 1s (**j**) of the series of CDs. Samples prepared with ethylenediamine (EDA), diethylenetriamine (DTEA), and triethylenetetramine (TETA) were named EDA CDs, DTEA CDs, and TETA CDs, respectively, whereas CDs prepared with deionized water without amine sources were named CS CDs.

the carbon chain of the amine modifier was extended. When the concentration of CDs reached 50 μg mL^{-1}, the antibacterial rate of EDA and DTEA CDs reached more than 90% in 1 h, while the antibacterial rate of TETA CDs reached 80% even at a relatively low concentration of 10 μg mL^{-1}, which indicates better antibacterial efficiency than shown in previous reports [54].

Interestingly, although the series of amine-modified CDs showed good antibacterial effects against *S. aureus*, they had almost no toxic effects on *B. subtilis*. Even when the concentration of TETA CDs was increased to 200 μg mL^{-1} or the concentration of *B. subtilis* was reduced to 10^3 CFU mL^{-1}, no significant inhibitory effects on *B. subtilis* were found (Fig. 2c). Therefore, amine-modified CDs with corn straw as a carbon source can be used as a highly effective bactericide that specifically targets and kills *S. aureus* while retaining *B. subtilis*.

However, the temperature of environmental water varies greatly throughout the year, especially in northern China, and research on the antibacterial activity of CDs as antibacterial disinfectants often focuses on 37 °C or room temperature (25 °C) [50,54–56]. There is little research on low-temperature antibacterial activity, which significantly restricts its practical application in water antibacterial disinfection. By testing the antibacterial activity of the series of amine-modified CDs at different temperatures (Fig. 2d), it was found that when the concentration of CDs was controlled at 50 μg mL^{-1} and the temperature was kept above 15 °C, the activity of EDA CDs was slightly reduced at 15 and 25 °C,

Table 1
Percentage of the functional groups in high-resolution XPS: C 1s, O 1s, and N 1s spectra of a series of CDs.

Percentage (%)	C 1s			O 1s			N 1s		
	C–C	C–O	C=O/C=N	C–OH/C–O–C	C=O	O–C=O	C=N	N–H	C–N
TETA CDs	43.4	33.3	23.4	84.9	12.2	2.9	90.4	9.6	–
DTEA CDs	54.2	38.0	7.9	94.3	3.2	2.5	90.7	9.3	–
EDA CDs	43.8	41.1	15.1	85.2	11.0	3.8	88.2	11.8	–
CS CDs	51.3	33.6	15.1	89.9	10.1	–	–	–	100

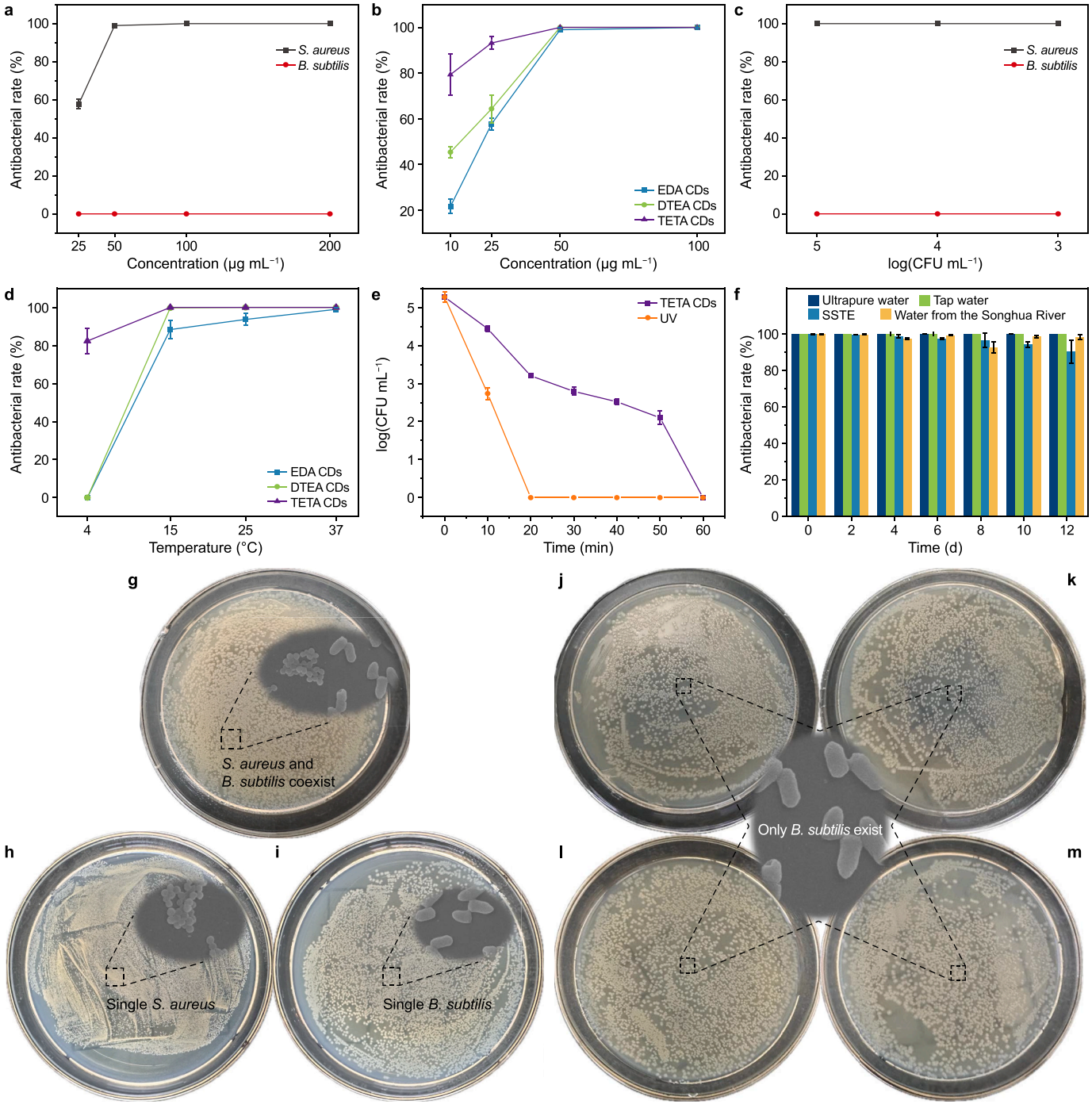

Fig. 2. **a**, Effect of EDA CD concentration on antibacterial rate of *S. aureus* and *B. subtilis* (10^5 colony-forming units (CFU), 37 °C, 1 h). **b**, Antibacterial rate of EDA CDs, DTEA CDs, and TETA CDs against *S. aureus*. (10^5 CFU, 37 °C, 1 h). **c**, Effect of bacterial concentration on the antibacterial rate of TETA CDs against *S. aureus* and *B. subtilis* (50 μg mL^{-1}, 37 °C, 1 h). **d**, Effect of temperature on antibacterial rate of CDs against *S. aureus*. (10^5 CFU, 50 μg mL^{-1}, 1 h). **e**, Growth curve of *S. aureus* under TETA CDs and ultraviolet (UV) treatment. **f**, Long-term antibacterial rate of TETA CDs. **g**–**m**, Selective antibacterial effects of TETA CDs in different water samples: control groups with *S. aureus* and *B. subtilis* coexist (**g**), single *S. aureus* (**h**), and single *B. subtilis* (**i**); test groups in ultrapure water (**j**), tap water (**k**), secondary sedimentation tank effluent (SSTE, **l**), and river water from the Songhua River (**m**) (10^5 CFU, TETA CDs concentration 50 μg mL^{-1}, 37 °C, 1 h). CDs: carbon dots. Samples prepared with ethylenediamine (EDA), diethylenetriamine (DTEA), and triethylenetetramine (TETA) were named EDA CDs, DTEA CDs, and TETA CDs, respectively.

while the activity of DTEA CDs and TETA CDs was not affected by temperature. When the temperature was dropped to 4 °C, the antibacterial activity of EDA and DTEA CDs was completely inhibited, while TETA CDs exhibited slightly reduced activity, with antibacterial activity dropping from 100% to 80%. This demonstrates that TETA CDs maintain a high antibacterial activity under low-temperature conditions, which can expand their application in actual water sterilization and disinfection.

To further evaluate the antibacterial activity of amine-modified CDs using TETA CDs as a representative, the antibacterial efficiency of TETA CDs was studied using a time-dynamic sterilization test (Fig. 2e). The number of live colonies decreased significantly with

the extension of contact time. The antibacterial efficiency reached 99% after 20 min, and the bacteria had been completely killed after 1 h. Although the efficiency is lower than that of traditional ultraviolet sterilization, which can kill bacteria within 20 min, complete exposure of a bacterial solution to ultraviolet light without shielding introduces many uncertainties into the sterilization process. Moreover, the ultraviolet (UV) inactivation of microorganisms is primarily attributed to DNA damage caused by the generation of cyclobutane pyrimidine dimers and 6-4 photoproducts, which interfere with genetic transcription and replication processes, ultimately leading to cell death. A critical limitation of UV disinfection is the capacity of inactivated microbes to repair such damage through photoreactivation and dark repair mechanisms, which can severely reduce disinfection effectiveness [57].

We expanded the antibacterial activity testing to Gram-negative bacteria *E. coli* and *P. aeruginosa* (Supplementary Fig. S3), showing that the TETA CDs exhibit no obvious toxicity toward *E. coli* and *P. aeruginosa* even at a relatively high concentration of 200 μg mL^{-1}. The long-term antibacterial performance and selective killing ability of TETA CDs in different water bodies (such as ultrapure water, tap water, secondary sedimentation tank effluent (SSTE), and river water from the Songhua River (Harbin, China)) were also investigated. TETA CDs were prepared into a 1 mg mL^{-1} stock solution, which was stored at room temperature (25 °C), to explore their long-term antibacterial performance (Fig. 2f). The TETA CDs exhibited excellent long-term stable antibacterial performance. Within 12 days, the antibacterial rate of TETA CDs reached 99% in ultrapure water, tap water, and river water from the Songhua River, while it decreased slightly in SSTE but remained above 90%. To this end, the antibacterial efficiency of TETA CDs in selectively killing *S. aureus* in actual water was further verified (Fig. 2g–m). It was found that after *S. aureus* and *B. subtilis* were mixed and treated with TETA CDs in different water samples for 1 h, the *S. aureus* could be selectively killed, and the physiological activity of *B. subtilis* was retained (Fig. 2i). Therefore, TETA CDs have good application potential in preventing *S. aureus* infections in environmental water, and we selected TETA CDs as a representative to further study their selective antibacterial mechanisms.

3.3. Selective antibacterial mechanisms of TETA CDs

As a natural biomass waste, corn straw itself has no antibacterial activity, and is even prepared into corn straw CDs. However, CDs prepared with amine modifiers derived from corn straw exhibit excellent, unique selective bactericidal properties that warrant further study. The antibacterial results show that TETA CDs can effectively kill the pathogenic bacteria *S. aureus* but have

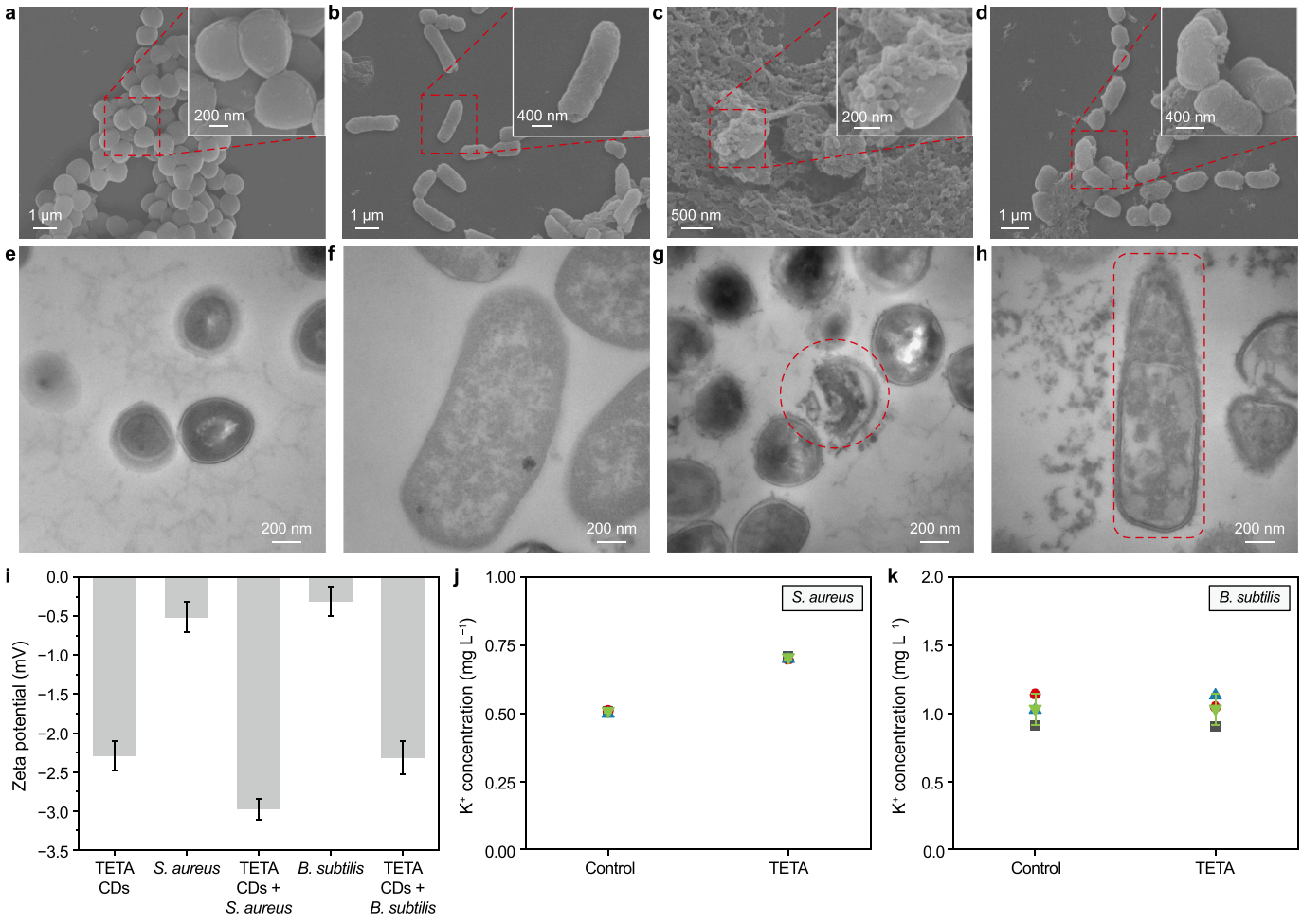

Fig. 3. a–d, Scanning electron microscopy images of S. aureus (**a,c**): **a**, control; **c**, TETA CDs treated, and B. subtilis (**b,d**): **b**, control; **d**, TETA CDs treated. **e–h**, TEM images of S. aureus (**e,g**): **e**, control; g, TETA CDs treated, and B. subtilis (**f,h**): **f**, control; **h**, TETA CDs treated. **i**, Zeta potential of different samples. **j-k**, K^+ concentration of *S. aureus* (**j**) and *B. subtilis* (**k**) solution, each treatment group was tested in triplicate.

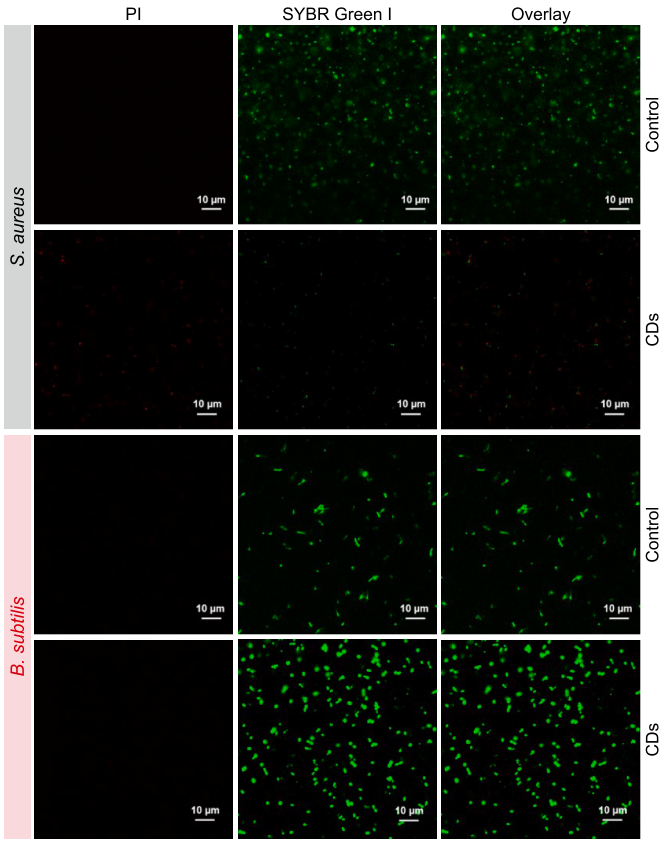

Fig. 4. Confocal laser scanning microscope images of *S. aureus* and *B. subtilis* solution treated with phosphate-buffered saline (control) and TETA CDs (CDs) (PI and SYBR Green I; 37 °C; 1 h). TETA: triethylenetetramine. CDs: carbon dots.

no effect on the probiotic *B. subtilis* in water. To investigate the antibacterial mechanism of TETA CDs, SEM was employed to visualize morphological changes in *S. aureus* and *B. subtilis* following treatment. Untreated control bacteria retained their characteristic morphologies: intact spherical cells for *S. aureus* and rod-like structures for *B. subtilis* (Fig. 3a and b) [58]. In contrast, *S. aureus* cells exposed to TETA CDs for 1 h (Fig. 3c) displayed significant membrane disruption, with CDs adhering to the cell surface, leading to structural collapse and deflation. These observations indicate progressive membrane damage and cell death. Conversely, treated *B. subtilis* cells (Fig. 3d) showed less CD adsorption, maintaining intact cell walls and regular rod shapes indistinguishable from untreated controls, confirming their metabolic viability [54].

The TEM images of the bacteria show the distribution of the bacteria and CDs. Compared with the control *S. aureus* (Fig. 3e), plenty of CDs were adsorbed on the cell membrane surface of *S. aureus* after treatment with TETA CDs (Fig. 3g), which destroyed the bacterial cell membrane structure. In contrast, the cell structure of the treated *B. subtilis* (Fig. 3h) showed a thicker cell wall than that of the control group (Fig. 3f), which can reduce or even prevent the adsorption of CDs on the cell structure, thereby preventing its destruction.

Zeta potential plays an important role in evaluating the adsorption performance of CDs [59]. To further evaluate the selective adsorption of CDs on both bacteria, we tested the TETA CDs and bacterial fluid in zeta potential (Fig. 3i). Although TETA CDs and both bacteria are negatively charged, SEM and TEM observations revealed that TETA CDs can still be adsorbed on the cell membrane surface of *S. aureus*, demonstrating that its electrostatic repulsion is not its dominant adsorption process. After the TETA CDs were mixed with *S. aureus* and *B. subtilis*, the zeta potential of the mixed liquid of *B. subtilis* and TETA CDs was almost unaffected. The zeta potential of the mixed solution of *S. aureus* and TETA CDs was significantly reduced, from the original TETA CD zeta potential of −2.3 to −3.0 mV, indicating that TETA CDs adsorb on the cell membrane of *S. aureus* to cover their positive charge sites, changing the surface nucleus distribution and increasing the negative charge density of the system. The interaction between TETA CDs and *B. subtilis* was relatively weak and did not significantly change the surface charge distribution of TETA CDs due to differences in the cellular structures of the two bacteria [60]. These results suggest that membrane-targeted interactions between TETA CDs and bacterial cells may underlie their selective antibacterial activity.

K^+ is critical for intracellular homeostasis, governing pH regulation, osmotic balance, and membrane potential maintenance [61]. The destruction of the membrane structure may trigger the leakage of K^+ from the cell, thereby damaging a variety of physiological processes for bacteria [62]. In this regard, the changes in K^+ concentration before and after treatment of the two bacterial solutions were detected by ICP-OES (Fig. 3j and k). K^+ concentration in the *S. aureus* solution increased significantly following CD treatment, while the K^+ concentration in the *B. subtilis* solution exhibited almost no change. The CDs' ability to selectively destroy the cell structure of *S. aureus* without affecting the activity of *B. subtilis* further supports the above conclusion. This selective destruction of bacterial cell structure results in the selective sterilization of CDs.

To visualize the selective antibacterial activity of CDs, *S. aureus* and *B. subtilis* were stained with PI/SYBR Green I before and after treatment, and imaged using CLSM (Fig. 4) [63]. The untreated bacteria emitted strong green fluorescence with minimal red signals, indicating intact membranes and viable cells [64]. TETA CD-treated *S. aureus* exhibited reduced green fluorescence and intense red staining, reflecting membrane damage and cell death. *B. subtilis* retained its green fluorescence profile, indistinguishable from controls, confirming membrane integrity and metabolic activity even at high CD concentrations (1 mg mL^{-1}). These results demonstrate the ability of TETA CDs to selectively eliminate pathogenic *S. aureus* while preserving the probiotic *B. subtilis*, highlighting their potential for targeted antimicrobial applications.

To investigate the adsorption mechanism of CDs on bacterial cell membranes, their affinity toward the key structural components of bacterial membranes was evaluated. Bovine serum albumin (BSA; representing membrane proteins), SA (mimicking extracellular polysaccharides), and phosphatidyl ethanolamine (PE; a major phospholipid component) were selected as representative biomolecules to characterize CD–membrane interactions [65]. Through the sedimentation experiment (Fig. 5a), it was found that the mixed solution of polysaccharide and CDs settled at 5 h, much faster than PE and BSA (PE settled weakly at 11 h, while BSA had no obvious sediment), indicating that CDs preferentially interacted with polysaccharides and consequently formed larger hetero agglomerations, while the interaction between CDs and phospholipid and protein were weak or negligible. Subsequent antibacterial assays revealed that SA suppressed the antibacterial activity of the CDs. The inhibitory effect of SA on TETA CDs (Fig. 5b) was significantly higher than that of BSA ($p < 0.001$) and PE ($p < 0.01$), which was consistent with the results of the sedimentation test.

The zeta potential of the interaction between TETA CDs and the main components of the bacterial membrane was measured (Fig. 5c). It can be found that SA significantly altered the surface

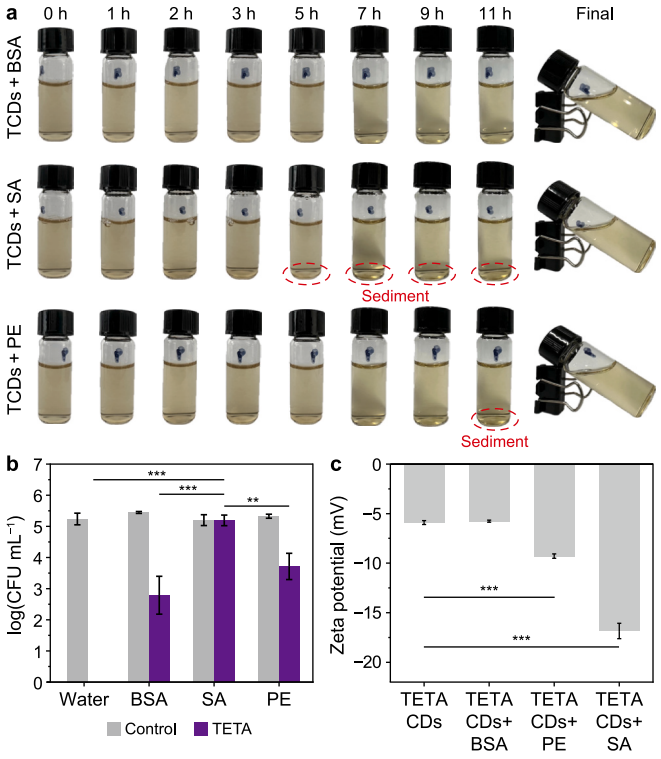

Fig. 5. **a**, Photographs of the sedimentation experiments. **b**, Antibacterial activity of characteristic substances with triethylenetetramine-derived carbon dots (TETA CDs concentration, 50 μg mL^{-1}; 37 °C; 1 h). **c**, Zeta potential of different characteristic substances with TETA CDs. $^{**}p < 0.01$, $^{***}p < 0.001$. BSA: bovine serum albumin; PE: phosphatidyl ethanolamine; SA: sodium alginate.

charge and distribution of TETA CDs through specific binding, whereas PE bound weakly to the CDs, and BSA failed to induce significant charge changes in TETA CDs. This conclusion is consistent with the results of the aforementioned sedimentation experiments and antibacterial inhibition assays, further demonstrating the preferential binding property of CDs to polysaccharides. This indicates that CDs preferentially bind to polysaccharide moieties on bacterial cell membranes, thereby disrupting membrane integrity and triggering apoptotic cell death. The selective adsorption of CDs to the polysaccharide structures on the cell membrane of *S. aureus* is key to the selective bactericidal properties of this series of CDs.

3.4. Antibacterial mechanism of TETA CDs

We chose ascorbic acid as an antioxidant to evaluate the ROS generation efficiency of CDs. We used physiological saline as the negative control and H_2O_2 (final concentration 10 mmol L^{-1}) as the positive control (Fig. 6a). After 1 h of treatment with AA, the AA degraded to different degrees, indicating that CDs mediated the production of ROS at differing efficiencies. The concentration of AA gradually decreased with the lengthening of the carbon chain of the amine modifier, corresponding to the antibacterial activity of three amine-modified CDs, which indicated that the oxidation ability of CDs toward AA gradually increased with the extension of the carbon chain of the amine modifier. This conclusion is consistent with the antibacterial efficiency results of the series of CDs.

We investigated the effect of the absence of O_2 on ROS production by CDs (Fig. 6b), and found that in the absence of O_2, the oxidation ability of the CDs was almost completely inhibited.

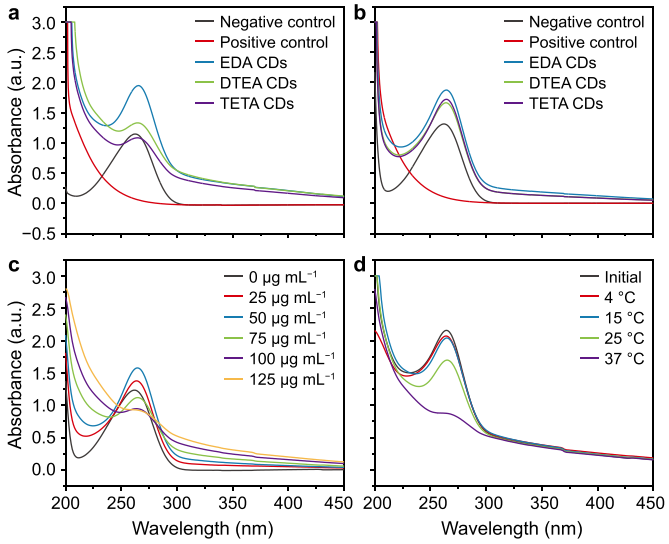

Fig. 6. Absorbance of ascorbic acid (AA) treated with different carbon dots (CDs). **a**, Presence of O_2. **b**, Absence of O_2. **c**, Absorbance of AA treated with different concentrations of TETA CDs (1 h). **d**, Absorbance of AA treated with different temperatures of TETA CDs (1 h; 100 μg mL^{-1}). Samples prepared with ethylenediamine (EDA), diethylenetriamine (DTEA), and triethylenetetramine (TETA) were named EDA CDs, DTEA CDs, and TETA CDs, respectively.

These results indicate that the ROS generation pathway of CDs necessitates the involvement of O_2. The observed ROS production exhibited a CDs dose-dependent relationship (Fig. 6c), suggesting that CDs function as excellent oxidases [66]. The oxidation ability of TETA CDs toward AA at different temperatures (4–37 °C) was also tested. As the temperature increased, the degradation ability of TETA CDs toward AA gradually increased (Fig. 6d), indicating that the production of ROS increased with rising temperature in the range of 4–37 °C. CDs capable of generating ROS have been demonstrated to circumvent bacterial resistance mechanisms through their ability to induce oxidative damage to multiple cellular macromolecules, including nucleic acids, proteins, and lipids [67]. This targeted strategy contrasts with conventional antibiotics, which selectively disrupt specific metabolic pathways, thereby offering a more robust solution to antimicrobial resistance.

To confirm the involvement of ROS in the bactericidal mechanism of CDs, we added radical quenchers, such as AA (1 mmol L^{-1}) [68], isopropyl alcohol (IPA; 1 mmol L^{-1}) [69], tert-butanol (TBA; 1 mmol L^{-1}), and L-histidine (1 mmol L^{-1}) [70]. Their addition attenuated the important role of ROS in the sterilization process (Fig. 7a). As a typical radical scavenger, AA can remove ·OH and $\cdot O_2^-$ free radicals, and the addition of AA significantly attenuated the antibacterial activity of CDs at both tested concentrations, indicating that ROS were produced in the reaction system [71]. IPA and TBA are both effective scavengers for ·OH, and the addition of IPA or TBA had no effect on the antibacterial rate of CDs, indicating that ·OH radicals were not produced or were not the main ROS generated by CDs during the antibacterial process. The $\cdot O_2^-$ radical is a latent ROS that affects the antibacterial activity of CDs. In the presence of L-histidine (Fig. 7a), a $^1O_2$ radical scavenger, the antibacterial rate of CDs to *S. aureus* decreased at 50 μg mL^{-1} but was essentially unaffected at 100 μg mL^{-1}, indicating that $^1O_2$ radicals were generated during the antibacterial process of CDs but were not the main ROS under these conditions. To further verify ROS generation, EPR spectroscopy was performed in the presence of ROS probes (Fig. 7b and c). The absorption signal of DMPO-$\cdot O_2^-$

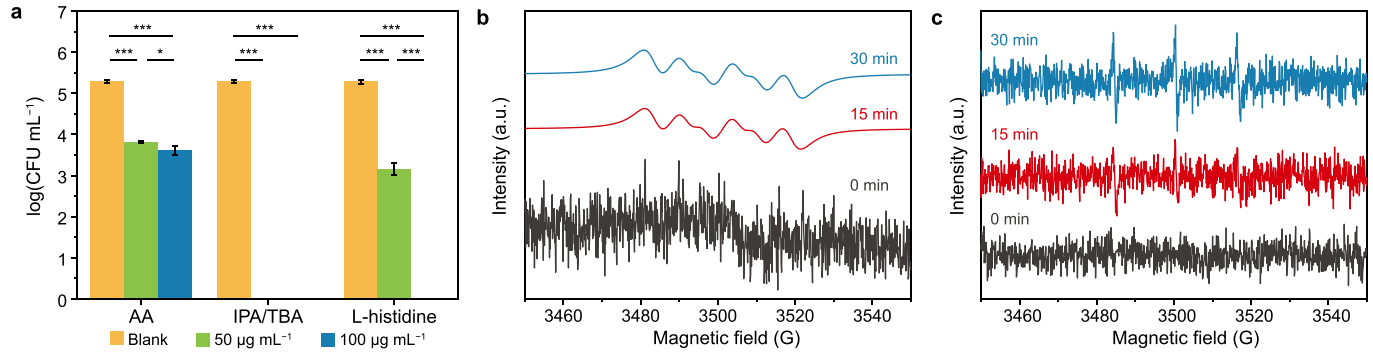

Fig. 7. **a**, Effects of different reactive oxygen species (ROS) quenchers on the antibacterial activity of TETA CDs. AA: ascorbic acid; IPA: isopropyl alcohol; TBA: tert-butanol. $*p < 0.05$, $**p < 0.01$, $***p < 0.001$. **b–c**, Electron paramagnetic resonance spectra of TETA CDs in the presence of 5,5-dimethyl-1-pyrroline N-oxide (DMPO, **b**) in methanol and 2,2,6,6-tetramethylpiperidine (TEMP, **c**) in water.

adduct observed at 15 and 30 min (Fig. 7b) confirmed the generation of $^1O_2$ (Fig. 7c), while the characteristic peak of 1:2:2:1 of hydroxyl was not detected (Supplementary Fig. S4), ruling out significant ·OH production. The quantification data in Supplementary Table S1 revealed that the spin density and molar concentration of $\cdot O_2^-$ were consistently greater than those of $^1O_2$, providing direct evidence for the superior bactericidal efficacy of $\cdot O_2^-$ radicals [72].

Finally, the intracellular ROS of *S. aureus* treated with different CDs were quantified using a DCFH-DA fluorescence assay. Under normal circumstances, the level of ROS in cells is controlled, and cells maintain the balance of ROS through antioxidant enzymes [73–75]. However, when cells are subjected to external environmental stressors such as ultraviolet radiation, pollutants, or certain drugs, the production of ROS may exceed the antioxidant capacity of cells, leading to oxidative stress and triggering cell damage and

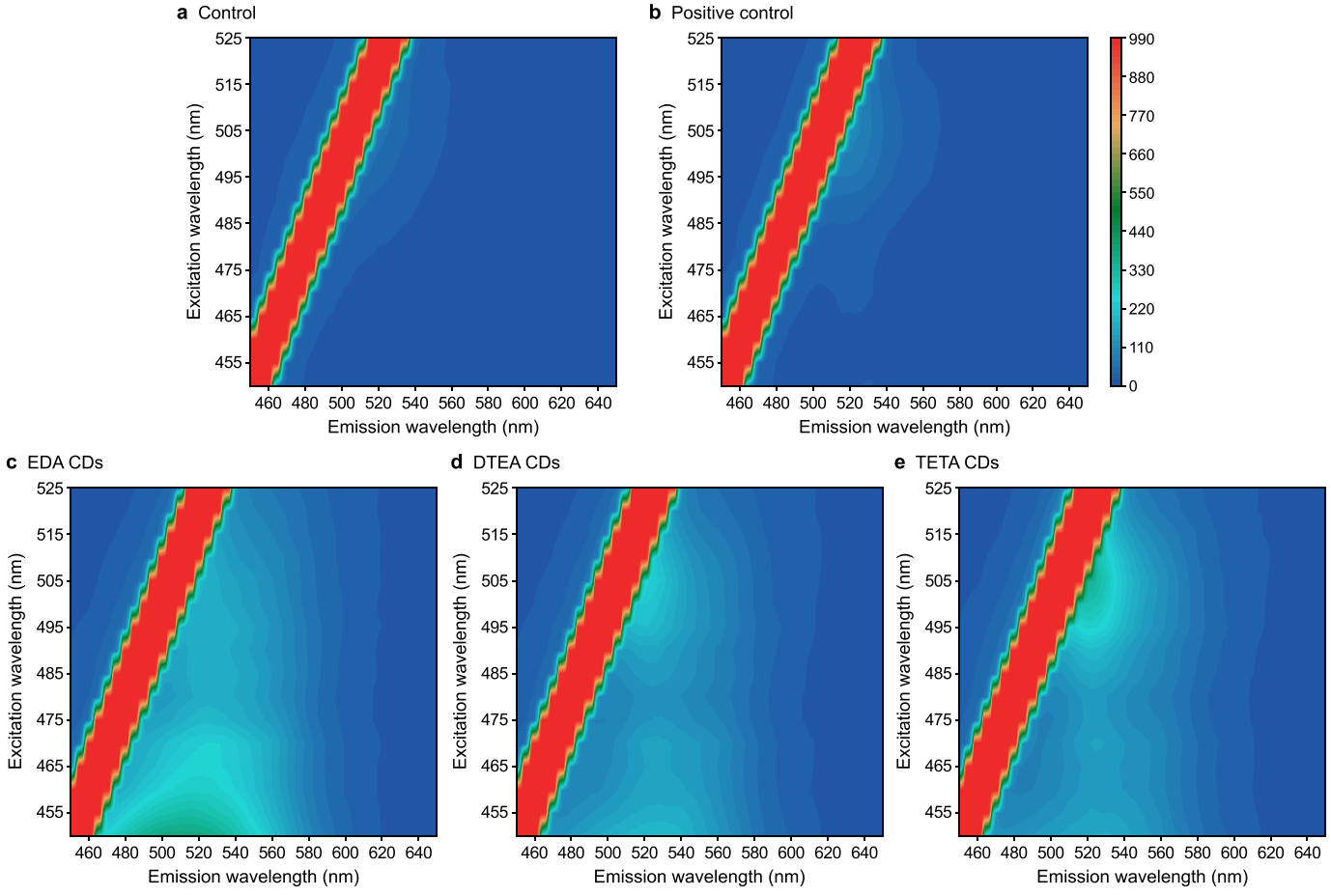

Fig. 8. Three-dimensional fluorescence spectra of *S. aureus* after treatment with a series of carbon dots (CDs). **a**, Control. **b**, Positive control. **c**, EDA CDs. **d**, DTEA CDs. **e**, TETA CDs. (CDs concentration, 50 μg mL^{-1}; 37 °C; 1 h). Samples prepared with ethylenediamine (EDA), diethylenetriamine (DTEA), and triethylenetetramine (TETA) were named EDA CDs, DTEA CDs, and TETA CDs, respectively.

apoptosis [76]. Amine-modified CDs significantly elevated the intracellular ROS levels in *S. aureus* (Fig. 8). Notably, ROS production in CD-treated bacteria was substantially higher than that induced by the positive control (10 mmol L^{-1} H_2O_2). The ROS-inducing capacity of the CD series correlated with the increasing carbon chain length of amine modifiers, indicating a dose-dependent relationship between modifier structure and antibacterial activity. This result corresponds to the AA oxidation ability and antibacterial activity of this series of CDs, demonstrating that the oxidation ability of CDs gradually increases with the extension of the carbon chain of the amine modifier. When the large amount of ROS produced exceeds the bacteria's ability to scavenge exogenous ROS, it leads to a continuous increase in the intracellular ROS level of the bacteria, and the bacteria gradually die [77,78].

These findings indicate the antimicrobial mechanisms of amine-modified biomass waste corn straw CDs, as schematically represented (Fig. 9). The structural retention mechanism posits that residual cellulose moieties on CD surfaces interact with amine modifiers, thereby preserving their active functional groups, which is beneficial to the adsorption and accumulation of CDs on the polysaccharide structure surface of the cell membrane of *S. aureus*, but does not appreciably adsorb to the cell membrane of *B. subtilis*. This targeted binding avoids significant damage to *B. subtilis* cell membranes, likely due to differences in the cellular structures of the two bacteria, and thus avoids interfering with a critical metabolic process for *B. subtilis* survival. More importantly, given that most ROS have an effective diffusion radius of less than 200 nm and a short half-life [79], only the ROS produced by CDs that selectively adsorb on the cell membrane of *S. aureus* can directly act on the cell membrane structure. This dual effect of adsorption-induced membrane adsorption and localized ROS attack damages the physical integrity of the cell membrane (evidenced by the SEM/TEM, zeta potential, and significant K^+ leakage, Fig. 3) and induces oxidative stress (CLSM and intracellular ROS of

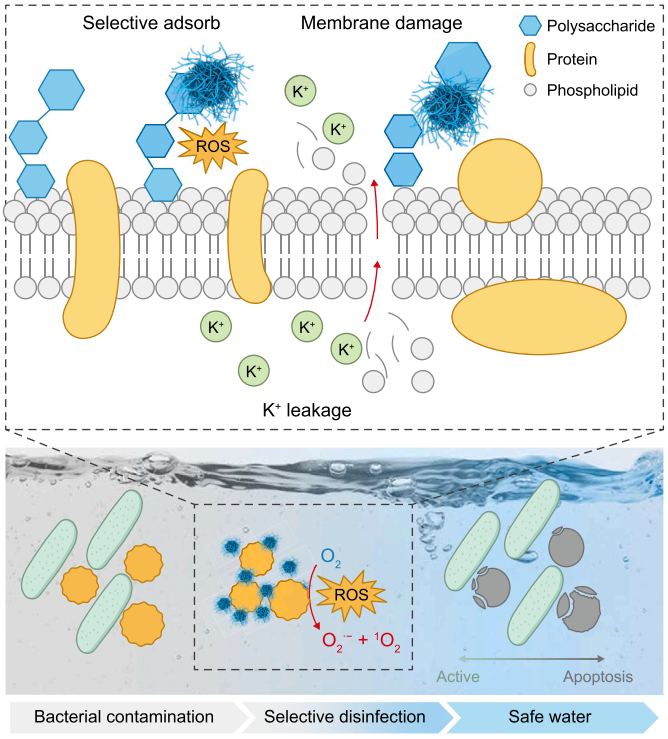

Fig. 9. Mechanism of the selective antibacterial mechanism of a series of carbon dots. ROS: reactive oxygen species.

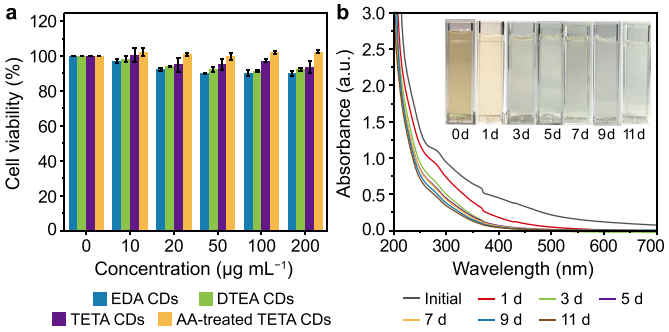

Fig. 10. a, Vitality of NIH 3T3 cells after different treatments. **b**, Ultraviolet–visible spectra of TETA CDs with different times of visible-light irradiation (25 °C; 1000 W m^{-2}). Inset photographs show the appearance of carbon dot (CD) solutions from Day 0 to Day 11. Samples prepared with ethylenediamine (EDA), diethylenetriamine (DTEA), and triethylenetetramine (TETA) were named EDA CDs, DTEA CDs, and TETA CDs, respectively. AA: ascorbic acid.

S. aureus, Figs. 4 and 8). These combined effects progressively impair cellular metabolic processes, leading to metabolic stagnation and eventual apoptosis [80]. Furthermore, with the extension of the carbon skeleton of the amine modifier, TETA CDs exhibit good oxidase-like activities, even at 4 °C, by generating $\cdot O_2^-$ and $^1O_2$ in the presence of O_2. We found that $\cdot O_2^-$ was the main ROS generated by TETA CDs via quantitative analysis of ROS spins. Ultimately, this synergy of selective adsorption, membrane damage, metabolic disruption, and ROS imbalance achieves the targeted killing of *S. aureus*.

Finally, the CCK-8 assay was employed to evaluate the effects of the series of CDs (EDA CDs, DTEA CDs, TETA CDs, and AA-treated TETA CDs) on the viability of NIH 3T3 cells, thereby assessing their potential environmental hazards (Fig. 10a) [81]. Within the tested concentration range (0–200 μg mL^{-1}), the cell viability of all CD-treated groups remained higher than 90%, generally approaching or even exceeding 100%. This indicates that these CDs exhibited negligible cytotoxicity toward NIH 3T3 cells under the experimental concentration conditions, demonstrating good biocompatibility and minimal environmental risks. The degradability of TETA CDs was also investigated to comprehensively evaluate their environmental impact. According to previous reports, CDs can be gradually decomposed into CO, CO_2, and H_2O under visible light irradiation, and the UV–Vis spectrum shows a flat line, indicating that organic residues basically disappear after 30 days [82]. The degradation of TETA CDs at different times was tested under the conditions of simulated sunlight conditions (1000 W m^{-2}) and at 25 °C (Fig. 10b). With prolonged light irradiation, the TETA-CD solution progressively faded from yellow to colorless over 11 days, and the intensity of its characteristic absorption peaks decreased gradually to disappear. This confirms that TETA CDs also possess excellent sunlight degradation ability, indicating that they have no persistence risk in natural aquatic environments and providing key support for the subsequent evaluation of their environmental safety.

4. Conclusion

This study presents an innovative strategy for the narrow-spectrum, selective killing of *S. aureus* from probiotic *B. subtilis* using amine-modified CDs synthesized from corn straw biomass waste via a one-step hydrothermal method. The CDs can be selectively adsorbed to the polysaccharide structure of the *S. aureus* cell membrane, which effectively destroys the cell membrane structure and increases the intracellular ROS of

S. aureus in the presence of oxygen, producing ROS, $\cdot O_2^-$, and $^1O_2$. Such behavior contributed to the selective killing of *S. aureus* without obvious toxicity to *B. subtilis*. Among the series of amine-modified CDs, the TETA CDs exhibited outstanding antibacterial efficiency with a relatively low concentration (50 μg mL^{-1}) and at low temperatures (4 °C), and showed a selective ability to kill *S. aureus* without affecting *B. subtilis* in natural water. Our approach emphasizes the use of waste and the efficient, selective killing of *S. aureus* across various water systems, including at low temperatures. The sustainable, low-cost, and highly effective narrow-spectrum antibacterial agent proposed in this study has the potential to replace traditional broad-spectrum antimicrobial agents. It exhibits excellent low-temperature antibacterial activity, making it suitable for water treatment in cold regions. Additionally, it can selectively kill *S. aureus* in complex aquatic environments while preserving probiotics, and can be applied in ecological water treatment to maintain microbial community balance, thereby paving the way for the development of eco-friendly, temperature-adaptive precision antibacterial technologies. This provides new avenues and insights for the utilization of CDs in water disinfection. Future research should focus on loading CDs onto the surface of water treatment membrane materials to construct a continuous-flow antibacterial water treatment system and systematically evaluate their practical application efficiency under continuous-flow conditions.

CRediT authorship contribution statement

Pengzhao Lv: Writing - Original Draft, Methodology, Investigation, Conceptualization. **Yu Jiang:** Validation, Supervision. **Jialin Wang:** Supervision. **Yige Shi:** Supervision. **Zhengda Lin:** Writing - Review & Editing. **Duo Wei:** Writing - Review & Editing, Investigation, Conceptualization. **Wei Zuo:** Writing - Review & Editing. **Jun Zhang:** Writing - Review & Editing, Validation, Resources, Funding Acquisition.

Data availability

All data generated or analyzed during this study are available within the paper and its Supplementary material files, or can be obtained from the corresponding author upon request.

Declaration of competing interest

The authors declare that they have no known competing financial interests or personal relationships that could have appeared to influence the work reported in this paper.

Acknowledgements

This study was supported by the National Key R&D Program of China (2023YFC3207400), the National Natural Science Foundation of China (52170028 and 22409040), the State Key Laboratory of Urban Water Resource and Environment, HIT (2023DX11), and the Heilongjiang Provincial S&T Program (HST2023GF003). The authors also appreciate the support of the Science Foundation of the National Engineering Research Center for Safe Disposal and Resource Recovery of Sludge (Z2024A014).

Appendix A. Supplementary data

Supplementary data to this article can be found online at https://doi.org/10.1016/j.ese.2025.100651.

References

[1] W. Zhou, M. Spoto, R. Hardy, C. Guan, E. Fleming, P.J. Larson, J.S. Brown, J. Oh, Host-specific evolutionary and transmission dynamics shape the functional diversification of Staphylococcus epidermidis in human skin, Cell 180 (3) (2020) 454–470 e18, https://doi.org/10.1016/j.cell.2020.01.006.
[2] R. Huang, Y. Tang, L. Luo, Thermochemistry of sulfur during pyrolysis and hydrothermal carbonization of sewage sludges, Waste Manag. 121 (2021) 276–285, https://doi.org/10.1016/j.wasman.2020.12.004.
[3] O.P. Abioye, V.T. Iroegu, S.A. Aransiola, Biodegradation of methyl red by Staphylococcus aureus isolated from waste dump site, J. Environ. Sci. Technol. 8 (3) (2015) 131–138, https://doi.org/10.3923/jest.2015.131.138.
[4] B. Cui, D. An, H. Li, X. Luo, H. Zhu, M. Li, X. Ai, J. Ma, W. Ali, C. Yan, Evaluating the threshold limit value of acceptable exposure concentration for exposure to bioaerosols in a wastewater treatment plant: reverse-quantitative microbial risk assessment and sensitivity analysis, J. Hazard. Mater. 452 (2023) 130687, https://doi.org/10.1016/j.jhazmat.2022.130687.
[5] A. Kozajda, K. Jezak, A. Kapsa, Airborne Staphylococcus aureus in different environments-a review, Environ. Sci. Pollut. Res. Int. 26 (34) (2019) 34741–34753, https://doi.org/10.1007/s11356-019-06557-1.
[6] K.W. Moon, E.H. Huh, H.C. Jeong, Seasonal evaluation of bioaerosols from indoor air of residential apartments within the metropolitan area in South Korea, Environ. Monit. Assess. 186 (4) (2014) 2111–2120, https://doi.org/10.1007/s10661-013-3521-8.
[7] G.Y. Fang, F.H. Wu, X.J. Mu, Y.J. Jiang, X.Q. Liu, Monitoring longitudinal antimicrobial resistance trends of Staphylococcus aureus strains worldwide over the past 100 years to decipher its evolution and transmission, J. Hazard. Mater. 465 (2023) 133136, https://doi.org/10.1016/j.jhazmat.2023.133136.
[8] X. Yu, Y. Ma, S. Liu, C. Qi, W. Zhang, W. Xiang, Z. Li, K. Yang, S. Duan, X. Du, J. Yu, Y. Xie, Z. Wang, W. Jiang, L. Zhang, X. Lin, Bacterial metabolism-triggered-chemiluminescence-based point-of-care testing platform for sensitive detection and photothermal inactivation of Staphylococcus aureus, Anal. Chim. Acta 1281 (2023) 341899, https://doi.org/10.1016/j.aca.2023.341899.
[9] M. Lou, S. Liu, C. Gu, H. Hu, Z. Tang, Y. Zhang, C. Xu, F. Li, The bioaerosols emitted from toilet and wastewater treatment plant: a literature review, Environ. Sci. Pollut. Res. Int. 28 (3) (2021) 2509–2521, https://doi.org/10.1007/s11356-020-11297-8.
[10] A. Vantarakis, S. Paparrodopoulos, P. Kokkinos, G. Vantarakis, K. Fragou, I. Detorakis, Impact on the quality of life when living close to a municipal wastewater treatment plant, J. Environ. Public Health 2016 (2016) 8467023, https://doi.org/10.1155/2016/8467023.
[11] X. Ding, C. Robbe-Masselot, X. Fu, R. Leonard, B. Marsac, C.J.G. Dauriat, A. Lepissier, H. Rytter, E. Ramond, M. Dupuis, D. Euphrasie, I. Dubail, C. Schimmich, X. Qin, J. Parraga, M. Leite-de-Moraes, A. Ferroni, B. Chassaing, I. Sermet-Gaudelus, A. Charbit, M. Coureuil, A. Jamet, Airway environment drives the selection of quorum sensing mutants and promote Staphylococcus aureus chronic lifestyle, Nat. Commun. 14 (1) (2023) 8135, https://doi.org/10.1038/s41467-023-43863-2.
[12] M. Steadmon, K. Ngiraklang, M. Nagata, K. Masga, K.L. Frank, Effects of water turbidity on the survival of Staphylococcus aureus in environmental fresh and brackish waters, Water Environ. Res. 95 (9) (2023) e10923, https://doi.org/10.1002/wer.10923.
[13] N.A. Travlou, D.A. Giannakoudakis, M. Algarra, A.M. Labella, E. Rodríguez-Castellón, T.J. Bandosz, S- and N-doped carbon quantum dots: surface chemistry dependent antibacterial activity, Carbon 135 (2018) 104–111, https://doi.org/10.1016/j.carbon.2018.04.018.
[14] S. Chernousova, M. Epple, Silver as antibacterial agent: ion, nanoparticle, and metal, Angew. Chem., Int. Ed. Engl. 52 (6) (2013) 1636–1653, https://doi.org/10.1002/anie.201205923.
[15] S. Buffet-Bataillon, P. Tattevin, M. Bonnaure-Mallet, A. Jolivet-Gougeon, Emergence of resistance to antibacterial agents: the role of quaternary ammonium compounds–a critical review, Int. J. Antimicrob. Agents 39 (5) (2012) 381–389, https://doi.org/10.1016/j.ijantimicag.2012.01.011.
[16] S.B. Levy, B. Marshall, Antibacterial resistance worldwide: causes, challenges and responses, Nat. Med. 10 (12 Suppl) (2004) S122–S129, https://doi.org/10.1038/nm1145.
[17] H. Sun, N. Gao, K. Dong, J. Ren, X. Qu, Graphene quantum dots-band-aids used for wound disinfection, ACS Nano 8 (6) (2014) 6202–6210, https://doi.org/10.1021/nn501640q.
[18] P. Li, S. Liu, W. Cao, G. Zhang, X. Yang, X. Gong, X. Xing, Low-toxicity carbon quantum dots derived from gentamicin sulfate to combat antibiotic resistance and eradicate mature biofilms, Chem. Commun. (Camb.) 56 (15) (2020) 2316–2319, https://doi.org/10.1039/c9cc09223d.
[19] P. Li, F. Han, W. Cao, G. Zhang, J. Li, J. Zhou, X. Gong, G. Turnbull, W. Shu, L. Xia, B. Fang, X. Xing, B. Li, Carbon quantum dots derived from lysine and arginine simultaneously scavenge bacteria and promote tissue repair, Appl. Mater. Today 19 (2020), https://doi.org/10.1016/j.apmt.2020.100601.
[20] H. Wang, M. Zhang, K. Wei, Y. Zhao, H. Nie, Y. Ma, Y. Zhou, H. Huang, Y. Liu, M. Shao, Z. Kang, Pyrrolic nitrogen dominated the carbon dot mimic oxidase activity, Carbon 179 (2021) 692–700, https://doi.org/10.1016/j.carbon.2021.04.061.
[21] J. Wu, T. Chen, S. Ge, W. Fan, H. Wang, Z. Zhang, E. Lichtfouse, T. Van Tran, R.K. Liew, M. Rezakazemi, R. Huang, Synthesis and applications of carbon

quantum dots derived from biomass waste: a review, Environ. Chem. Lett. 21 (6) (2023) 3393–3424, https://doi.org/10.1007/s10311-023-01636-9.
[22] W.B. Zhao, K.K. Liu, Y. Wang, F.K. Li, R. Guo, S.Y. Song, C.X. Shan, Antibacterial carbon dots: mechanisms, design, and applications, Adv. Healthcare Mater. 12 (23) (2023) e2300324, https://doi.org/10.1002/adhm.202300324.
[23] X. Zhao, L. Wang, S. Ren, Z. Hu, Y. Wang, One-pot synthesis of Forsythia@ carbon quantum dots with natural anti-wood rot fungus activity, Mater. Des. 206 (2021), https://doi.org/10.1016/j.matdes.2021.109800.
[24] L. Wu, Y. Gao, C. Zhao, D. Huang, W. Chen, X. Lin, A. Liu, L. Lin, Synthesis of curcumin-quaternized carbon quantum dots with enhanced broad-spectrum antibacterial activity for promoting infected wound healing, Biomater. Adv. 133 (2022) 112608, https://doi.org/10.1016/j.msec.2021.112608.
[25] Z. Wang, L. Sheng, X. Yang, J. Sun, Y. Ye, S. Geng, D. Ning, J. Zheng, M. Fan, Y. Zhang, X. Sun, Natural biomass-derived carbon dots as potent antimicrobial agents against multidrug-resistant bacteria and their biofilms, Sustain. Mater. Technol. 36 (2023), https://doi.org/10.1016/j.susmat.2023.e00584.
[26] K. Huang, X. Fan, R. Ashby, H. Ngo, Structure-activity relationship of antibacterial bio-based epoxy polymers made from phenolic branched fatty acids, Prog. Org. Coating 155 (2021), https://doi.org/10.1016/j.porgcoat.2021.106228.
[27] S. Jyakhwo, V. Bocharova, N. Serov, A. Dmitrenko, V.V. Vinogradov, SelTox: discovering the capacity of selectively antimicrobial nanoparticles for targeted eradication of pathogenic bacteria, Adv. Mater. Technol.-Us (2024) 2400458, https://doi.org/10.1002/admt.202400458.
[28] C. Kang, S. Tao, F. Yang, B. Yang, Aggregation and luminescence in carbonized polymer dots, Aggregate 3 (2) (2022), https://doi.org/10.1002/agt2.169.
[29] S. Zheng, L. Feng, Z. Hu, J. Li, H. Zhu, X. Ma, Study on the corrosion inhibition of biomass carbon quantum dot self- aggregation on Q235 steel in hydrochloric acid, Arab. J. Chem. 16 (4) (2023), https://doi.org/10.1016/j.arabjc.2023.104605.
[30] L. Mu, W. Wu, J. Huang, H. Peng, Y. Song, J. Tao, G. Chen, Simultaneous synthesis of carbon quantum dots and hydrothermal biochar from corn straw through hydrothermal treatment, Ind. Crop. Prod. 219 (2024), https://doi.org/10.1016/j.indcrop.2024.119026.
[31] S.S. Jones, P. Sahatiya, S. Badhulika, One step, high yield synthesis of amphiphilic carbon quantum dots derived from chia seeds: a solvatochromic study, New J. Chem. 41 (21) (2017) 13130–13139, https://doi.org/10.1039/c7nj03513f.
[32] F. Du, L. Zhang, L. Zhang, M. Zhang, A. Gong, Y. Tan, J. Miao, Y. Gong, M. Sun, H. Ju, C. Wu, S. Zou, Engineered gadolinium-doped carbon dots for magnetic resonance imaging-guided radiotherapy of tumors, Biomaterials 121 (2017) 109–120, https://doi.org/10.1016/j.biomaterials.2016.07.008.
[33] X. Zhao, J. Chen, F. Chen, X. Wang, Q. Zhu, Q. Ao, Surface characterization of corn stalk superfine powder studied by FTIR and XRD, Colloids Surf. B Biointerfaces 104 (2013) 207–212, https://doi.org/10.1016/j.colsurfb.2012.12.003.
[34] C. Lou, Y. Zhou, A. Yan, Y. Liu, Extraction cellulose from corn-stalk taking advantage of pretreatment technology with immobilized enzyme, RSC Adv. 12 (2) (2021) 1208–1215, https://doi.org/10.1039/d1ra07513f.
[35] A.A. Yakout, R.H. El-Sokkary, M.A. Shreadah, O.G. Abdel Hamid, Removal of Cd(II) and Pb(II) from wastewater by using triethylenetetramine functionalized grafted cellulose acetate-manganese dioxide composite, Carbohydr. Polym. 148 (2016) 406–414, https://doi.org/10.1016/j.carbpol.2016.04.038.
[36] A. Alemdar, M. Sain, Isolation and characterization of nanofibers from agricultural residues – wheat straw and soy hulls, Bioresour. Technol. 99 (6) (2008) 1664–1671, https://doi.org/10.1016/j.biortech.2007.04.029.
[37] X.F. Sun, F. Xu, R.C. Sun, P. Fowler, M.S. Baird, Characteristics of degraded cellulose obtained from steam-exploded wheat straw, Carbohydr. Res. 340 (1) (2005) 97–106, https://doi.org/10.1016/j.carres.2004.10.022.
[38] B.M. Cherian, L.A. Pothan, T. Nguyen-Chung, G. Mennig, M. Kottaisamy, S. Thomas, A novel method for the synthesis of cellulose nanofibril whiskers from banana fibers and characterization, J. Agric. Food Chem. 56 (14) (2008) 5617–5627, https://doi.org/10.1021/jf8003674.
[39] J. Zhang, Y. Li, Y. Dai, T. Lin, H. Shao, Y. Liu, X. Liu, Three-dimensional porous hydrogel based on hyperbranched polyethyleneimine functionalized apple pomace derived cellulose for efficient removal of methyl orange, Chem. Eng. J. 456 (2023), https://doi.org/10.1016/j.cej.2022.140995.
[40] L. Lai, G. Huang, X. Wang, J. Weng, Solvothermal syntheses of hollow carbon microspheres modified with –NH2 and –OH groups in one-step process, Carbon 48 (11) (2010) 3145–3156, https://doi.org/10.1016/j.carbon.2010.04.053.
[41] H. Ding, J.S. Wei, H.M. Xiong, Nitrogen and sulfur co-doped carbon dots with strong blue luminescence, Nanoscale 6 (22) (2014) 13817–13823, https://doi.org/10.1039/c4nr04267k.
[42] M. Liu, L. Huang, X. Xu, X. Wei, X. Yang, X. Li, B. Wang, Y. Xu, L. Li, Z. Yang, Copper doped carbon dots for addressing bacterial biofilm formation, wound infection, and tooth staining, ACS Nano 16 (6) (2022) 9479–9497, https://doi.org/10.1021/acsnano.2c02518.
[43] M. Wan, J. Zhou, H. Yang, X. Dai, Y. Zheng, Z. Xia, L. Wang, Covalently N-Doped MXene quantum dots for highly stable fluorescent Cu2+ ion sensor, ACS Appl. Nano Mater. 5 (8) (2022) 11715–11722, https://doi.org/10.1021/acsanm.2c02699.
[44] K.-K. Niu, C.-Q. Ma, R.-Z. Dong, H. Liu, S.-S. Yu, L.-B. Xing, Nitrogen-doped carbon dots as photocatalysts for organic synthesis: effect of nitrogen content on catalytic activity, Nano Res. 17 (6) (2024) 4825–4833, https://doi.org/10.1007/s12274-024-6451-6.
[45] V. Fernandez, D. Morgan, P. Bargiela, N. Fairley, J. Baltrusaitis, Combining PCA and nonlinear fitting of peak models to re-evaluate C 1s XPS spectrum of cellulose, Appl. Surf. Sci. 614 (2023), https://doi.org/10.1016/j.apsusc.2022.156182.
[46] Q. Yang, J. Duan, W. Yang, X. Li, J. Mo, P. Yang, Q. Tang, Nitrogen-doped carbon quantum dots from biomass via simple one-pot method and exploration of their application, Appl. Surf. Sci. 434 (2018) 1079–1085, https://doi.org/10.1016/j.apsusc.2017.11.040.
[47] Y. Wang, P. Poldorn, Y. Wongnongwa, S. Jungsuttiwong, C. Chen, L. Yu, Z. Wang, L. Shi, Y. Zhao, S. Yuan, Cobalt(II)-Hexaazatriphenylene hexacarbonitrile coordination compounds based cathode materials with high capacity and long cycle stability, Adv. Funct. Mater. 32 (16) (2022), https://doi.org/10.1002/adfm.202111043.
[48] W. Luo, Z. Bai, Y. Zhu, Comparison of Co(ii) adsorption by a crosslinked carboxymethyl chitosan hydrogel and resin: behaviour and mechanism, New J. Chem. 41 (9) (2017) 3487–3497, https://doi.org/10.1039/c6nj03837a.
[49] S.E. Mackay, F. Malherbe, D.S. Eldridge, Quaternary amine functionalized chitosan for enhanced adsorption of low concentration phosphate to remediate environmental eutrophication, Colloids Surf. A Physicochem. Eng. Asp. 653 (2022), https://doi.org/10.1016/j.colsurfa.2022.129984.
[50] C. Zhao, X. Wang, L. Wu, W. Wu, Y. Zheng, L. Lin, S. Weng, X. Lin, Nitrogen-doped carbon quantum dots as an antimicrobial agent against Staphylococcus for the treatment of infected wounds, Colloids Surf. B 179 (2019) 17–27, https://doi.org/10.1016/j.colsurfb.2019.03.042.
[51] Q. Meng, S. Wu, C. Shen, Polyethylenimine-grafted-corncob as a multifunctional biomaterial for removing heavy metal ions and killing bacteria from water, Ind. Eng. Chem. Res. 59 (39) (2020) 17476–17482, https://doi.org/10.1021/acs.iecr.9b06606.
[52] Y. Mori, Y. Kuwano, S. Tomokiyo, N. Kuroyanagi, K. Odahara, Inhibitory effects of Moso bamboo (phyllostachys heterocycla f. pubescens) extracts on phytopathogenic bacterial and fungal growth, Wood Sci. Technol. 53 (1) (2018) 135–150, https://doi.org/10.1007/s00226-018-1063-5.
[53] Y. Ilieva, M.M. Zaharieva, A.D. Kroumov, H. Najdenski, Antimicrobial and ecological potential of chlorellaceae and scenedesmaceae with a focus on wastewater treatment and industry, Fermentation 10 (7) (2024), https://doi.org/10.3390/fermentation10070341.
[54] M. Yu, X. Guo, H. Lu, P. Li, R. Huang, C. Xu, X. Gong, Y. Xiao, X. Xing, Carbon dots derived from folic acid as an ultra-succinct smart antimicrobial nanosystem for selective killing of S. aureus and biofilm eradication, Carbon 199 (2022) 395–406, https://doi.org/10.1016/j.carbon.2022.07.065.
[55] Z. Mao, X. Peng, H. Chen, Sunlight propelled two-dimensional nanorobots with enhanced mechanical damage of bacterial membrane, Water Res. 235 (2023) 119900, https://doi.org/10.1016/j.watres.2023.119900.
[56] C. Zhao, L. Wu, X. Wang, S. Weng, Z. Ruan, Q. Liu, L. Lin, X. Lin, Quaternary ammonium carbon quantum dots as an antimicrobial agent against gram-positive bacteria for the treatment of MRSA-infected pneumonia in mice, Carbon 163 (2020) 70–84, https://doi.org/10.1016/j.carbon.2020.03.009.
[57] P. Duque-Sarango, N. Delgado-Armijos, L. Romero-Martínez, V. Pinos-Vélez, Assessing the potential of ultraviolet irradiation for inactivating waterborne fungal spores: kinetics and photoreactivation studies, Front. Environ. Sci. 11 (2023), https://doi.org/10.3389/fenvs.2023.1212807.
[58] P. Lv, L. Zhu, Y. Yu, W. Wang, G. Liu, H. Lu, Effect of NaOH concentration on antibacterial activities of Cu nanoparticles and the antibacterial mechanism, Mater. Sci. Eng., C 110 (2020) 110669, https://doi.org/10.1016/j.msec.2020.110669.
[59] B.N. Tafese, T. Ganesh, A. Solomon, B. Sundararaju, N. Garg, B. Alebachew, Efficient adsorptive removal of methylene blue dye from aqueous solution using eragrostis teff biomass-derived nitrogen and phosphorus-codoped carbon quantum dots, Langmuir 40 (1) (2024) 72–83, https://doi.org/10.1021/acs.langmuir.3c01813.
[60] M. Zajac, J. Kotynska, G. Zambrowski, J. Breczko, P. Deptula, M. Ciesluk, M. Zambrzycka, I. Swiecicka, R. Bucki, M. Naumowicz, Exposure to polystyrene nanoparticles leads to changes in the zeta potential of bacterial cells, Sci. Rep. 13 (1) (2023) 9552, https://doi.org/10.1038/s41598-023-36603-5.
[61] P. Zhang, Y. Qiu, Y. Wang, L. Xiao, S. Yu, M. Shi, Y. Ni, R.J. Miron, Y. Pu, Y. Zhang, Nanoparticles promote bacterial antibiotic tolerance via inducing hyperosmotic stress response, Small 18 (19) (2022) e2105525, https://doi.org/10.1002/smll.202105525.
[62] K. Xing, Y. Xing, Y. Liu, Y. Zhang, X. Shen, X. Li, X. Miao, Z. Feng, X. Peng, S. Qin, Fungicidal effect of chitosan via inducing membrane disturbance against Ceratocystis fimbriata, Carbohydr. Polym. 192 (2018) 95–103, https://doi.org/10.1016/j.carbpol.2018.03.053.
[63] X. Lin, Y. Fang, Z. Hao, H. Wu, M. Zhao, S. Wang, Y. Liu, Bacteria-triggered multifunctional hydrogel for localized chemodynamic and low-temperature photothermal sterilization, Small 17 (51) (2021) e2103303, https://doi.org/10.1002/smll.202103303.
[64] M.T. Sim, Z.Y. Ee, Y.H. Lim, T.S. Sia, D.T.K. Ong, J.S.C. Koay, B.T. Goh, Y.S. Yong, K.C. Aw, S.T. Tan, W.C. Gan, Instant disinfecting face masks utilizing electroporation powered by respiration-driven triboelectric nanogenerators, Adv. Funct. Mater. (2024), https://doi.org/10.1002/adfm.202410062.
[65] S. Yin, D.P. Linklater, Z. Li, S. Zhao, S. He, S. Xiang, L. Sun, L. Han, L. Wen, S. Juodkazis, E.P. Ivanova, L. Jiang, K. Sun, Translocation of pyrimidine derivative-capped gold nanoparticles via membrane ion channels induce Pseudomonas aeruginosa and Staphylococcus aureus cell death, ACS Mater.

Lett. 6 (2) (2023) 418–426, https://doi.org/10.1021/acsmaterialslett.3c01326.
[66] X. Shen, W. Liu, X. Gao, Z. Lu, X. Wu, X. Gao, Mechanisms of oxidase and superoxide dismutation-like activities of gold, silver, platinum, and palladium, and their alloys: a general way to the activation of molecular oxygen, J. Am. Chem. Soc. 137 (50) (2015) 15882–15891, https://doi.org/10.1021/jacs.5b10346.
[67] F. Vatansever, W.C. de Melo, P. Avci, D. Vecchio, M. Sadasivam, A. Gupta, R. Chandran, M. Karimi, N.A. Parizotto, R. Yin, G.P. Tegos, M.R. Hamblin, Antimicrobial strategies centered around reactive oxygen species–bactericidal antibiotics, photodynamic therapy, and beyond, FEMS Microbiol. Rev. 37 (6) (2013) 955–989, https://doi.org/10.1111/1574-6976.12026.
[68] A.D. Bokare, R.C. Chikate, C.V. Rode, K.M. Paknikar, Effect of surface chemistry of Fe-Ni nanoparticles on mechanistic pathways of azo dye degradation, Environ. Sci. Technol. 41 (21) (2007) 7437–7443, https://doi.org/10.1021/es071107q.
[69] X.J. Wang, Y. Long, C.W. Wei, S.Q. Gao, Y.W. Lin, Peroxidase activity of a Cu-Fe bimetallic hydrogel and applications for colorimetric detection of ascorbic acid, Phys. Chem. Chem. Phys. 26 (2) (2024) 1077–1085, https://doi.org/10.1039/d3cp05403a.
[70] X. Liu, Y. Chen, Y. Yao, Q. Bai, Z. Wu, Iodine-doped carbon fibers as an efficient metal-free catalyst to activate peroxymonosulfate for the removal of organic pollutants, Catal. Sci. Technol. 8 (21) (2018) 5482–5489, https://doi.org/10.1039/c8cy01537f.
[71] F. Zhou, C. Lu, Y. Yao, L. Sun, F. Gong, D. Li, K. Pei, W. Lu, W. Chen, Activated carbon fibers as an effective metal-free catalyst for peracetic acid activation: implications for the removal of organic pollutants, Chem. Eng. J. 281 (2015) 953–960, https://doi.org/10.1016/j.cej.2015.07.034.
[72] K. Wu, X.Y. Liu, P.W. Cheng, Y.L. Huang, J. Zheng, M. Xie, W. Lu, D. Li, Linker engineering for reactive oxygen species generation efficiency in ultra-stable nickel-based metal-organic frameworks, J. Am. Chem. Soc. 145 (34) (2023) 18931–18938, https://doi.org/10.1021/jacs.3c05585.
[73] H. Zhao, R. Zhang, X. Yan, K. Fan, Superoxide dismutase nanozymes: an emerging star for anti-oxidation, J. Mater. Chem. B 9 (35) (2021) 6939–6957, https://doi.org/10.1039/d1tb00720c.
[74] H. Sepasi Tehrani, A.A. Moosavi-Movahedi, Catalase and its mysteries, Prog. Biophys. Mol. Biol. 140 (2018) 5–12, https://doi.org/10.1016/j.pbiomolbio.2018.03.001.
[75] L. Flohe, S. Toppo, L. Orian, The glutathione peroxidase family: discoveries and mechanism, Free Radic. Biol. Med. 187 (2022) 113–122, https://doi.org/10.1016/j.freeradbiomed.2022.05.003.
[76] S.Y. Kim, C. Park, H.J. Jang, B.O. Kim, H.W. Bae, I.Y. Chung, E.S. Kim, Y.H. Cho, Antibacterial strategies inspired by the oxidative stress and response networks, J. Microbiol. 57 (3) (2019) 203–212, https://doi.org/10.1007/s12275-019-8711-9.
[77] J.A. Imlay, Where in the world do bacteria experience oxidative stress? Environ. Microbiol. 21 (2) (2019) 521–530, https://doi.org/10.1111/1462-2920.14445.
[78] B. Ezraty, A. Gennaris, F. Barras, J.F. Collet, Oxidative stress, protein damage and repair in bacteria, Nat. Rev. Microbiol. 15 (7) (2017) 385–396, https://doi.org/10.1038/nrmicro.2017.26.
[79] A. Vaishampayan, E. Grohmann, Antimicrobials functioning through ROS-mediated mechanisms: current insights, Microorganisms 10 (1) (2021), https://doi.org/10.3390/microorganisms10010061.
[80] P. Hou, T. Yang, H. Liu, Y.F. Li, C.Z. Huang, An active structure preservation method for developing functional graphitic carbon dots as an effective antibacterial agent and a sensitive pH and Al(iii) nanosensor, Nanoscale 9 (44) (2017) 17334–17341, https://doi.org/10.1039/c7nr05539k.
[81] X. Sun, S. Luo, L. Zhang, Y. Miao, G. Yan, Photodynamic antibacterial activity of oxidase-like nanozyme based on long-lived room-temperature phosphorescent carbon dots, Food Chem. 434 (2024) 137541, https://doi.org/10.1016/j.foodchem.2023.137541.
[82] H. Li, J. Huang, Y. Song, M. Zhang, H. Wang, F. Lu, H. Huang, Y. Liu, X. Dai, Z. Gu, Z. Yang, R. Zhou, Z. Kang, Degradable carbon dots with broad-spectrum antibacterial activity, ACS Appl. Mater. Interfaces 10 (32) (2018) 26936–26946, https://doi.org/10.1021/acsami.8b08832.